Hindawi
Shock and Vibration
Volume 2017, Article ID 9301876, 15 pages
https://doi.org/10.1155/2017/9301876

Research Article

Time-Varying Wind Load Identification Based on Minimum-Variance Unbiased Estimation

Huili Xue, Kun Lin, Yin Luo, and Hongjun Liu

Shenzhen Graduate School, Harbin Institute of Technology, Shenzhen 518055, China

Correspondence should be addressed to Hongjun Liu; liuhongjun@hit.edu.cn

Received 22 March 2017; Revised 27 July 2017; Accepted 14 August 2017; Published 12 October 2017

Academic Editor: Marc Thomas

A minimum-variance unbiased estimation method is developed to identify the time-varying wind load from measured responses. The formula derivation of recursive identification equations is obtained in state space. The new approach can simultaneously estimate the entire wind load and the unknown structural responses only with limited measurement of structural acceleration response. The fluctuating wind speed process is investigated by the autoregressive (AR) model method in time series analysis. The accuracy and feasibility of the inverse approach are numerically investigated by identifying the wind load on a twenty-story shear building structure. The influences of the number and location of accelerometers are examined and discussed. In order to study the stability of the proposed method, the effects of the errors in crucial factors such as natural frequency and damping ratio are discussed through detailed parametric analysis. It can be found from the identification results that the proposed method can identify the wind load from limited measurement of acceleration responses with good accuracy and stability, indicating that it is an effective approach for estimating wind load on building structures.

1. Introduction

Wind load is one of the main lateral loads for civil engineering structures. For high-rise buildings, super-tall buildings, high towers, large span bridges, and so forth, wind load is the main design load. Therefore, the research of the wind effect on wind-sensitive structures has become a main topic for wind engineering researchers. In the design process of most structures, wind load varies depending on the basic wind pressure, and the coefficient of wind pressure varies with height, terrain conditions, coefficient of the shape of the structure, and the effect of the fluctuating wind components [1]. Therefore, it is difficult to calculate the actual wind load based on the wind load design code accurately. At present, wind tunnel tests are usually used to determine the wind-induced vibration and the wind load of the structures, especially for structures with a complex shape. However, the difficulties of accurately reproducing the characteristics of the model, the characteristics of terrain, and the characteristics of incident turbulence limit the accuracy of the wind tunnel tests. The field measurement method is considered to be the most reliable approach to determine the wind effects on prototype structures. However, with the limitation of the measurement equipment and measurement methods, real-time measurement of wind load on the structures is difficult to achieve by field measurement. In comparison, measurement of acceleration and displacement responses is easier and more accurate than that of force. Therefore, it is necessary to establish a method for time-varying wind load identification from measured structural responses.

The external load identified from the measurement responses of a structure is one of the classical inverse problems. The inverse problems mainly study the magnitude of the unknown load [2], the magnitude and location of the unknown load [3], and moving load [4]. Sanchez and Benaroya overviewed the load identification techniques [5]. They grouped the load identification techniques into three categories: direct, regularization, and probabilistic/statistical. The direct methods formulate the inverse problem with direct use of the physical or mathematical model and these methods can be performed in the time domain or the frequency domain analysis. Regularization methods can be utilized to overcome the ill-posed problem with additional physical or mathematical conditions [6–8]. Probabilistic or statistical

methods were employed by a probabilistic or statistical perspective to gain the unknown loads [9–11].

In recent years, several methods have been used to estimate the wind load on structures. Simonian developed the dynamic programming filter method for inverse problems and applied it in wind engineering [12, 13]. Chen and Li proposed a general statistical average algorithm to estimate unknown wind load with unknown structural parameters and they validated this method through numerical analysis of an existing twelve-story structure [14]. Kang and Lo estimated the wind load on an elevated tower and they also obtained the value of the ground vibration based on the discretized governing equations [15]. Law et al. developed a regularization method to obtain the unknown wind load based on structural displacement or strain responses, and this method was numerically validated by identifying the wind load on a 50 m guyed mast [16]. Hwang et al. utilized limited measured responses to identify the modal wind load based on Kalman filter method [17, 18]. Klinkov and Fritzen identified the wind loads on a 5 MW wind energy plant with a nonlinear observer and implemented the wind load reconstruction technique as a unit into the prototype structural health monitoring system [19]. Zhi et al. developed the Kalman filter method to estimate the wind load on super-tall buildings with limited structural responses. The effects of the type of wind-induced response, the covariance matrix of noise, errors of structural modal parameters, and the number of vibration modes were investigated through a detailed parametric study [20, 21]. Gillijns and Moor addressed simultaneously estimating the state and the unknown input method based on the minimum-variance unbiased estimation in 2007 [22, 23] and to the best of the authors' knowledge it has not been applied to wind load identification. Several studies observed that identification of the wind load from structural acceleration responses was relatively more stable and robust [17, 18]. Meanwhile, the measurement technology of structural acceleration responses is advanced and capable of high precision. In this study, the authors aim to estimate wind load from limited measurement of structural acceleration responses based on the minimum-variance unbiased estimation method for the first time, which provides a novel approach for wind load estimation.

In this paper, a time-varying wind load identification method is developed based on the minimum-variance unbiased estimation algorithm [22, 23]. The wind loads are identified from limited measurement of structural acceleration responses in the time domain with a recursive formula. The accuracy of the method is validated through comparison between the estimated and the exact wind load. Furthermore, the effects of key factors such as the number of accelerometers, the location of accelerometers, and the errors of structural modal parameters are studied and analyzed. The aim of this study is to verify the inverse method as an effective tool for predicting the wind load on building structures.

2. Wind Load Identification from Structural Responses

2.1. Wind Load Identification Based on Minimum-Variance Unbiased Estimation Scheme. The second-order differential equation of motion of an n-degree-of-freedom (DOF) building structure could be expressed as

$$\mathbf{M}\ddot{\mathbf{x}}(t) + \mathbf{C}\dot{\mathbf{x}}(t) + \mathbf{K}\mathbf{x}(t) = \mathbf{F}(t), \tag{1}$$

in which $\mathbf{M}$, $\mathbf{C}$, and $\mathbf{K}$ are $n \times n$ mass, damping, and stiffness matrices of the building structure, respectively. $\ddot{\mathbf{x}}(t)$, $\dot{\mathbf{x}}(t)$, and $\mathbf{x}(t)$ are $n \times 1$ structural acceleration, velocity, and displacement response vectors, respectively. $\mathbf{F}(t)$ is the $n \times 1$ wind load vector.

Consider a state vector that consists of structural displacement and velocity, which can be expressed as

$$\mathbf{Z}(t) = \left[\mathbf{x}^{\mathbf{T}}(t) \;\; \dot{\mathbf{x}}^{\mathbf{T}}(t)\right]^{T}. \tag{2}$$

The first-order differential equation of (2) can be represented as follows:

$$\begin{aligned}\frac{d\mathbf{Z}(t)}{dt} &= \begin{bmatrix} \dot{\mathbf{x}}^{T}(t) \\ \mathbf{M}^{-1}\left(\mathbf{F}(t) - \mathbf{K}\mathbf{x}(t) - \mathbf{C}\dot{\mathbf{x}}(t)\right)\end{bmatrix} \\ &= \begin{bmatrix} \mathbf{0}_{n\times n} & \mathbf{I}_{n\times n} \\ -\mathbf{M}^{-1}\mathbf{K} & -\mathbf{M}^{-1}\mathbf{C}\end{bmatrix}\begin{bmatrix}\mathbf{x}(t) \\ \dot{\mathbf{x}}(t)\end{bmatrix} + \begin{bmatrix}\mathbf{0}_{n\times n} \\ -\mathbf{M}^{-1}\end{bmatrix}\mathbf{F}(t).\end{aligned} \tag{3}$$

By substituting $(\mathbf{Z}_{k+1} - \mathbf{Z}_k)/\Delta t = d\mathbf{Z}(k\Delta t)/dt$, in which Δt is denoted as the sampling interval, into (3), one can obtain

$$\mathbf{Z}_{k+1} = \mathbf{A}_k\mathbf{Z}_k + \mathbf{B}_k\mathbf{F}_k, \tag{4}$$

where

$$\begin{aligned}\mathbf{A}_k &= \left(\mathbf{I}_{2n\times 2n} + \Delta t\begin{bmatrix}\mathbf{0}_{n\times n} & \mathbf{I}_{n\times n} \\ -\mathbf{M}^{-1}\mathbf{K} & -\mathbf{M}^{-1}\mathbf{C}\end{bmatrix}\right), \\ \mathbf{B}_k &= \Delta t\begin{bmatrix}\mathbf{0}_{n\times n} \\ -\mathbf{M}^{-1}\end{bmatrix}.\end{aligned} \tag{5}$$

The measurement equation associated with (1) at time $t = k \times \Delta t$ can be given as

$$\mathbf{y}_{k+1} = \mathbf{D}_{k+1}\mathbf{Z}_{k+1} + \mathbf{G}_{k+1}\mathbf{F}_{k+1} + \mathbf{v}_{k+1}, \tag{6}$$

where $\mathbf{y}_{k+1} = \ddot{\mathbf{x}}$ is the $n \times 1$ measurement vector which can be obtained from the measured acceleration responses. $\mathbf{D}_{k+1} = \left[-\mathbf{M}^{-1}\mathbf{K} \;\; -\mathbf{M}^{-1}\mathbf{C}\right]$ and $\mathbf{G}_{k+1} = \left[-\mathbf{M}^{-1}\right]$ are system matrices. $\mathbf{v}_{k+1}$ is an $n \times 1$ Gaussian measurement noise vector with zero mean and covariance matrix $\mathbf{R}_{k+1}\delta_{k+1} = E(\mathbf{v}_{k+1}\mathbf{v}_{k+1}^{T})$, where δ_{k+1} is the Kronecker delta.

Let $\widehat{\mathbf{Z}}_{k|k}$ and $\widehat{\mathbf{F}}_k$ denote the optimal unbiased estimates of $\mathbf{Z}_k$ and $\mathbf{F}_k$ at time $t = k \times \Delta t$, respectively. Then, the a priori estimation state $\widehat{\mathbf{Z}}_{k+1|k}$ at time $t = (k+1) \times \Delta t$ is given by

$$\widehat{\mathbf{Z}}_{k+1|k} = \mathbf{A}_k\widehat{\mathbf{Z}}_{k|k} + \mathbf{B}_k\widehat{\mathbf{F}}_k. \tag{7}$$

It should be noted that $\widehat{\mathbf{Z}}_{k+1|k}$ is the unbiased estimate of $\mathbf{Z}_{k+1}$ because $E(\widehat{\mathbf{Z}}_{k|k}) = E(\mathbf{Z}_k)$ and $E(\widehat{\mathbf{F}}_k) = E(\mathbf{F}_k)$; then, $E(\mathbf{Z}_{k+1}) = E(\widehat{\mathbf{Z}}_{k+1|k})$ can be obtained from (4). The a priori

estimate error of state vector $\mathbf{Z}_{k+1}$ at $t = (k+1) \times \Delta t$ can be calculated as follows:

$$\begin{aligned}\boldsymbol{\varepsilon}_{\mathbf{Z},k+1|k} &= \mathbf{Z}_{k+1} - \mathbf{Z}_{k+1|k} \\ &= \mathbf{A}_k \mathbf{Z}_k + \mathbf{B}_k \mathbf{F}_k - \left(\mathbf{A}_k \widehat{\mathbf{Z}}_{k|k} + \mathbf{B}_k \widehat{\mathbf{F}}_k\right) \\ &= \mathbf{A}_k \boldsymbol{\varepsilon}_{\mathbf{Z},k|k} + \mathbf{B}_k \boldsymbol{\varepsilon}_{\mathbf{F},k|k},\end{aligned} \tag{8}$$

with $\boldsymbol{\varepsilon}_{\mathbf{Z},k|k} = \mathbf{Z}_k - \widehat{\mathbf{Z}}_{k|k}$ and $\boldsymbol{\varepsilon}_{\mathbf{F},k|k} = \mathbf{F}_k - \widehat{\mathbf{F}}_k$.

The a priori estimation error covariance of state vector denoted as $\mathbf{P}_{\mathbf{Z},k+1|k}$ can be obtained by

$$\begin{aligned}\mathbf{P}_{\mathbf{Z},k+1|k} &= E\left(\boldsymbol{\varepsilon}_{\mathbf{Z},k+1|k} \boldsymbol{\varepsilon}_{\mathbf{Z},k+1|k}^T\right) \\ &= \begin{bmatrix}\mathbf{A}_k & \mathbf{B}_k\end{bmatrix} \begin{bmatrix}\mathbf{P}_{\mathbf{Z},k|k} & \mathbf{P}_{\mathbf{ZF},k|k} \\ \mathbf{P}_{\mathbf{FZ},k|k} & \mathbf{P}_{\mathbf{F},k|k}\end{bmatrix} \begin{bmatrix}\mathbf{A}_k^T \\ \mathbf{B}_k^T\end{bmatrix},\end{aligned} \tag{9}$$

in which $\mathbf{P}_{\mathbf{Z},k|k} = E(\boldsymbol{\varepsilon}_{\mathbf{Z},k|k} \boldsymbol{\varepsilon}_{\mathbf{Z},k|k}^T)$, $\mathbf{P}_{\mathbf{F},k|k} = E(\boldsymbol{\varepsilon}_{\mathbf{F},k|k} \boldsymbol{\varepsilon}_{\mathbf{F},k|k}^T)$, and $\mathbf{P}_{\mathbf{FZ},k|k} = \mathbf{P}_{\mathbf{ZF},k|k}^T = E(\boldsymbol{\varepsilon}_{\mathbf{F},k|k} \boldsymbol{\varepsilon}_{\mathbf{Z},k|k}^T)$.

Based on (6), one can obtain

$$\mathbf{y}_{k+1} - \mathbf{D}_{k+1} \widehat{\mathbf{Z}}_{k+1|k} = \mathbf{G}_{k+1} \mathbf{F}_{k+1} + \mathbf{H}_{k+1}, \tag{10}$$

where $\mathbf{H}_{k+1} = \mathbf{D}_{k+1} \boldsymbol{\varepsilon}_{\mathbf{Z},k+1|k} + \mathbf{v}_{k+1}$. The expected value of $\mathbf{H}_{k+1}$ denoted as $\widetilde{\mathbf{R}}_{k+1}$ can be calculated as

$$\widetilde{\mathbf{R}}_{k+1} = E\left(\mathbf{H}_{k+1} \mathbf{H}_{k+1}^T\right) = \mathbf{D}_{k+1} \mathbf{P}_{\mathbf{Z},k+1|k} \mathbf{D}_{k+1}^T + \mathbf{R}_{k+1}. \tag{11}$$

Solving (10) by the weighted least square method (WLS) with weighting matrix $\widetilde{\mathbf{R}}_{k+1}^{-1}$, the optimal unbiased estimates of unknown wind load $\mathbf{F}_{k+1}$ can be obtained as

$$\widehat{\mathbf{F}}_{k+1} = \mathbf{K}_{\mathbf{F},k+1} \left(\mathbf{y}_{k+1} - \mathbf{D}_{k+1} \widehat{\mathbf{Z}}_{k+1|k}\right), \tag{12}$$

where $\mathbf{K}_{\mathbf{F},k+1}$ is the gain matrix of wind load estimation and it is given by

$$\mathbf{K}_{\mathbf{F},k+1} = \left(\mathbf{G}_{k+1}^T \widetilde{\mathbf{R}}_{k+1}^{-1} \mathbf{G}_{k+1}\right)^{-1} \mathbf{G}_{k+1}^T \widetilde{\mathbf{R}}_{k+1}^{-1}. \tag{13}$$

Based on (6) and (12), the estimate error of unknown wind load can be calculated as follows:

$$\begin{aligned}\boldsymbol{\varepsilon}_{\mathbf{F},k+1} &= \mathbf{F}_{k+1} - \widehat{\mathbf{F}}_{k+1} \\ &= \left(\mathbf{I}_{n \times n} - \mathbf{K}_{\mathbf{F},k+1} \mathbf{G}_{k+1}\right) \mathbf{F}_{k+1} \\ &\quad - \mathbf{K}_{\mathbf{F},k+1} \mathbf{D}_{k+1} \boldsymbol{\varepsilon}_{\mathbf{Z},k+1|k} - \mathbf{K}_{\mathbf{F},k+1} \mathbf{v}_{k+1}.\end{aligned} \tag{14}$$

It should be noted that the estimation of state vector $\mathbf{Z}_k$ and the unknown wind load vector is unbiased; that is, $E(\boldsymbol{\varepsilon}_{\mathbf{Z},k+1|k}) = \mathbf{0}$ and $E(\boldsymbol{\varepsilon}_{\mathbf{F},k+1}) = \mathbf{0}$. Then, one can obtain

$$\mathbf{K}_{\mathbf{F},k+1} \mathbf{G}_{k+1} = \mathbf{I}_{n \times n}. \tag{15}$$

Equation (14) can be rewritten as

$$\boldsymbol{\varepsilon}_{\mathbf{F},k+1|k+1} = -\mathbf{K}_{\mathbf{F},k+1} \mathbf{H}_{k+1}. \tag{16}$$

The estimation error covariance of unknown wind load vector denoted as $\mathbf{P}_{\mathbf{F},k+1|k+1}$ can be calculated as

$$\begin{aligned}\mathbf{P}_{\mathbf{F},k+1|k+1} &= E\left(\boldsymbol{\varepsilon}_{\mathbf{F},k+1|k+1} \boldsymbol{\varepsilon}_{\mathbf{F},k+1|k+1}^T\right) \\ &= \left(\mathbf{G}_{k+1}^T \widetilde{\mathbf{R}}_{k+1}^{-1} \mathbf{G}_{k+1}\right)^{-1}.\end{aligned} \tag{17}$$

The form of the a posteriori estimation state $\widehat{\mathbf{Z}}_{k+1|k+1}$ at time $t = (k+1) \times \Delta t$ is defined as follows:

$$\widehat{\mathbf{Z}}_{k+1|k+1} = \widehat{\mathbf{Z}}_{k+1|k} + \widetilde{\mathbf{K}}_{Z,k+1} \left(\mathbf{y}_{k+1} - \mathbf{D}_{k+1} \widehat{\mathbf{Z}}_{k+1|k}\right), \tag{18}$$

in which $\widetilde{\mathbf{K}}_{\mathbf{Z},k+1}$ is the defined gain matrix of state estimation at time $t = (k+1) \times \Delta t$.

Based on (4), (6), and (18), the a posteriori estimate error of state vector $\mathbf{Z}_{k+1}$ at time $t = (k+1) \times \Delta t$ can be calculated as

$$\begin{aligned}\boldsymbol{\varepsilon}_{\mathbf{Z},k+1|k+1} &= \left(\mathbf{I}_{2n \times 2n} - \widetilde{\mathbf{K}}_{\mathbf{Z},k+1} \mathbf{D}_{k+1}\right) \boldsymbol{\varepsilon}_{\mathbf{Z},k+1|k} \\ &\quad - \widetilde{\mathbf{K}}_{\mathbf{Z},k+1} \mathbf{G}_{k+1} \mathbf{F}_{k+1} - \widetilde{\mathbf{K}}_{\mathbf{Z},k+1} \mathbf{v}_{k+1}.\end{aligned} \tag{19}$$

It should be noted that the unbiased estimation of state vector requires that $E(\boldsymbol{\varepsilon}_{\mathbf{Z},k+1|k}) = \mathbf{0}$ and $E(\boldsymbol{\varepsilon}_{\mathbf{Z},k+1|k+1}) = \mathbf{0}$. From (19), we can obtain the unbiased condition as follows:

$$\widetilde{\mathbf{K}}_{\mathbf{Z},k+1} \mathbf{G}_{k+1} = 0. \tag{20}$$

Then, the a posteriori estimate error of state vector $\mathbf{Z}_{k+1}$ at time $t = (k+1) \times \Delta t$ can be rewritten as

$$\begin{aligned}\boldsymbol{\varepsilon}_{\mathbf{Z},k+1|k+1} &= \left(\mathbf{I}_{2n \times 2n} - \widetilde{\mathbf{K}}_{\mathbf{Z},k+1} \mathbf{D}_{k+1}\right) \boldsymbol{\varepsilon}_{\mathbf{Z},k+1|k} \\ &\quad - \widetilde{\mathbf{K}}_{\mathbf{Z},k+1} \mathbf{v}_{k+1}.\end{aligned} \tag{21}$$

Similarly, the a posteriori estimate error covariance of state vector at time $t = (k+1) \times \Delta t$ can be obtained as

$$\begin{aligned}\mathbf{P}_{\mathbf{Z},k+1|k+1} &= E\left(\boldsymbol{\varepsilon}_{\mathbf{Z},k+1|k+1} \boldsymbol{\varepsilon}_{\mathbf{Z},k+1|k+1}^T\right) \\ &= \left(\mathbf{I}_{2n \times 2n} - \widetilde{\mathbf{K}}_{\mathbf{Z},k+1} \mathbf{D}_{k+1}\right) \\ &\quad \cdot \mathbf{P}_{\mathbf{Z},k+1|k} \left(\mathbf{I}_{2n \times 2n} - \widetilde{\mathbf{K}}_{\mathbf{Z},k+1} \mathbf{D}_{k+1}\right)^T \\ &\quad + \widetilde{\mathbf{K}}_{\mathbf{Z},k+1} \mathbf{R}_{k+1} \widetilde{\mathbf{K}}_{\mathbf{Z},k+1}^T.\end{aligned} \tag{22}$$

To obtain the minimum-variance unbiased estimation of state vector, the gain matrix $\widetilde{\mathbf{K}}_{\mathbf{Z},k+1}$ is calculated by minimizing the state estimation error covariance $\mathbf{P}_{\mathbf{Z},k+1|k+1}$ under the unbiased condition shown in (20). The gain matrix $\widetilde{\mathbf{K}}_{\mathbf{Z},k+1}$ is given by

$$\widetilde{\mathbf{K}}_{\mathbf{Z},k+1} = \mathbf{K}_{\mathbf{Z},k+1} \left(\mathbf{I}_{n \times n} - \mathbf{G}_{k+1} \mathbf{K}_{\mathbf{F},k+1}\right), \tag{23}$$

in which

$$\mathbf{K}_{\mathbf{Z},k+1} = \mathbf{P}_{\mathbf{Z},k+1|k} \mathbf{D}_{k+1}^T \widetilde{\mathbf{R}}_{k+1}^{-1}. \tag{24}$$

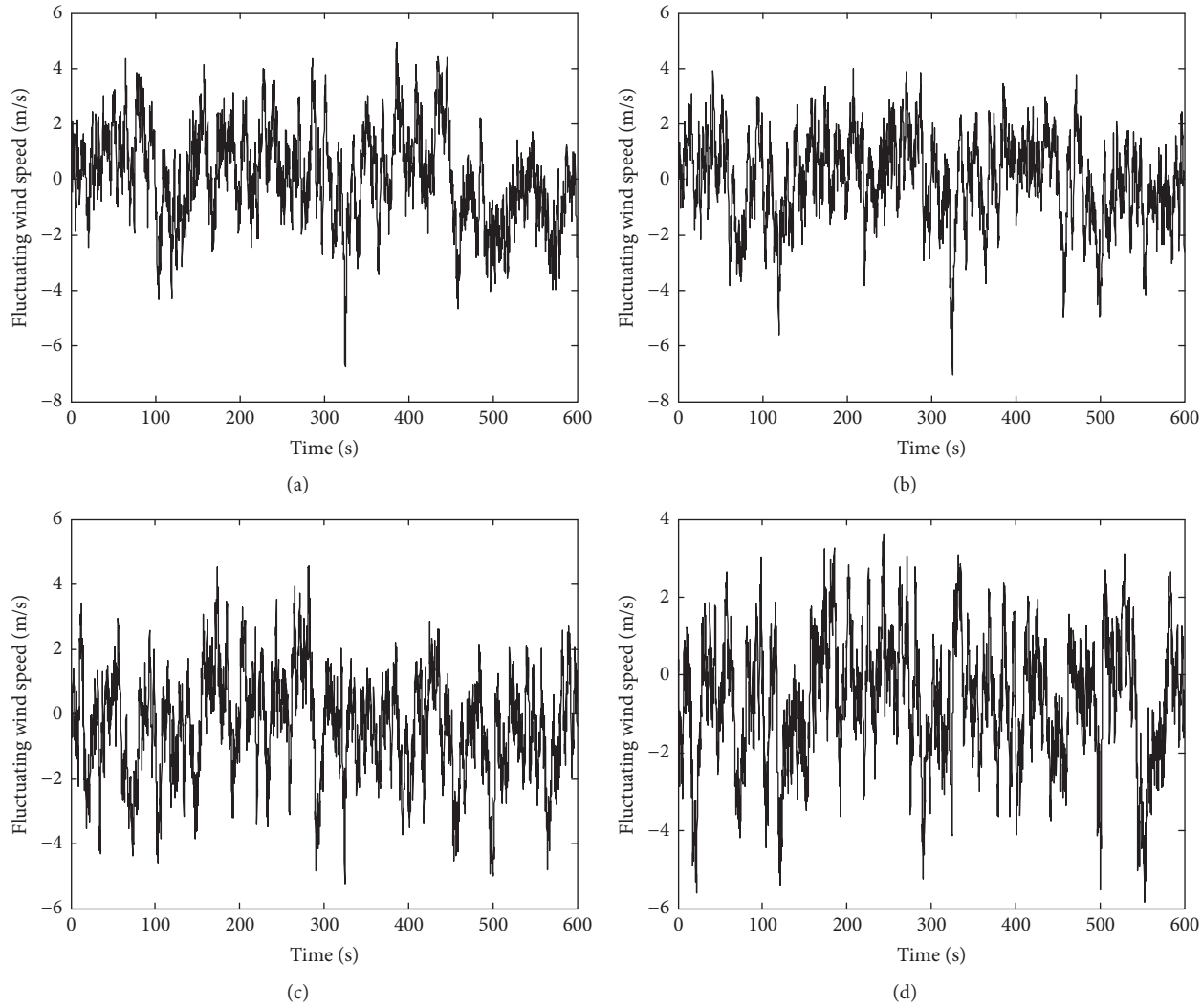

Figure 1: Simulated fluctuating wind speed. (a) On the 5th floor; (b) on the 10th floor; (c) on the 15th floor; (d) on the 20th floor.

By substituting (23) into (18) and (22), respectively, we can obtain the following expression:

$$\begin{aligned}\widehat{\mathbf{Z}}_{k+1|k+1} &= \widehat{\mathbf{Z}}_{k+1|k} + \mathbf{K}_{\mathbf{Z},k+1}\left(\mathbf{y}_{k+1} - \mathbf{D}_{k+1}\widehat{\mathbf{Z}}_{k+1|k} - \mathbf{G}_{k+1}\widehat{\mathbf{F}}_{k+1}\right),\\ \mathbf{P}_{\mathbf{Z},k+1|k+1} &= \mathbf{P}_{\mathbf{Z},k+1|k} - \mathbf{K}_{\mathbf{Z},k+1}\left(\widetilde{\mathbf{R}}_{k+1} - \mathbf{G}_{k+1}\mathbf{P}_{\mathbf{F},k+1}\mathbf{G}_{k+1}^{T}\right)\mathbf{K}_{\mathbf{Z},k+1}^{T}.\end{aligned} \tag{25}$$

Using (16) and (21), the expression of $\mathbf{P}_{\mathbf{ZF},k+1|k+1}$ and $\mathbf{P}_{\mathbf{FZ},k+1|k+1}$ at time $t = (k+1) \times \Delta t$ can be calculated as

$$\mathbf{P}_{\mathbf{ZF},k+1|k+1} = \mathbf{P}_{\mathbf{FZ},k+1|k+1}^{T} = -\mathbf{K}_{\mathbf{Z},k+1}\mathbf{G}_{k+1}\mathbf{P}_{\mathbf{F},k+1|k+1}. \tag{26}$$

It can be found that the recursive part of the filter includes three parts: time update, estimation of the unknown wind load, and measurement update. The time update equations include (7) and (9). The equations for estimating the unknown wind load include (11), (13), (12), and (17). The measurement update equations include (24) to (26). Take note that the measurement update is in the form of classical Kalman filter, except that the input in each time step is replaced by the optimal estimation. Additionally, we can find that the Kalman filter could be obtained if $\mathbf{B}_k = \mathbf{0}$ and $\mathbf{G}_k = \mathbf{0}$.

2.2. Wind Load Identification in Modal Space. In the previous section, the wind load identification method is applicable when the acceleration responses on each story can be measured. However, due to the drawbacks of measurement techniques, the complete measurement of structural acceleration response is limited in practical application. In addition, the response of a tall building under wind load is dominated by the first few modes. Hence, the estimation approach introduced in the previous section can be applied in modal space.

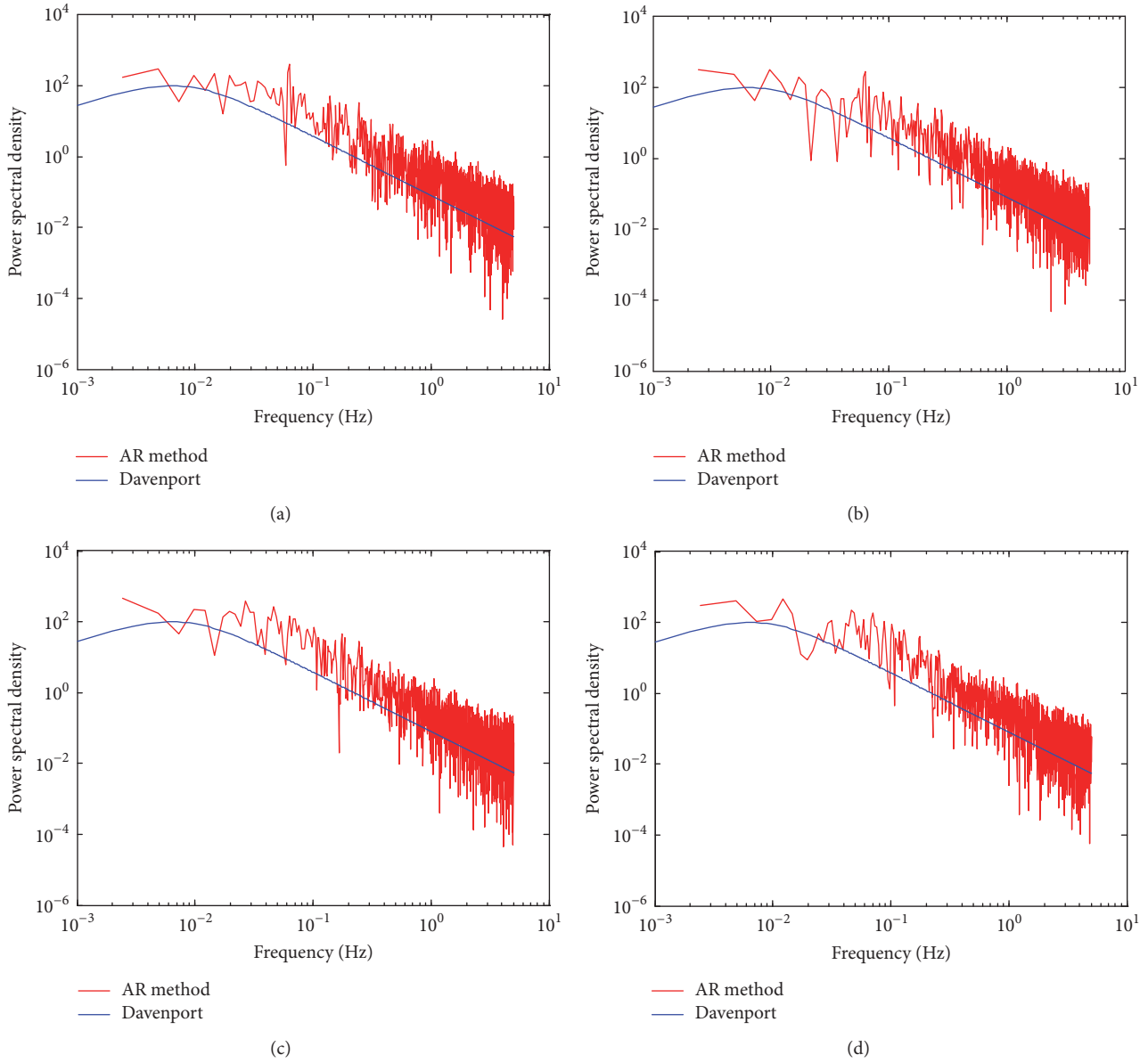

FIGURE 2: Comparison of power spectral density between simulated and Davenport spectra. (a) On the 5th floor; (b) on the 10th floor; (c) on the 15th floor; (d) on the 20th floor.

If the acceleration responses of all DOFs are measured, the acceleration can be shown as follows:

$$\ddot{\mathbf{x}}_{\mathbf{n}\times 1} = \Phi_{\mathbf{n}\times\mathbf{n}}\ddot{\mathbf{Y}}_{\mathbf{n}\times 1}, \tag{27}$$

in which $\Phi_{\mathbf{n}\times\mathbf{n}}$ is the $n\times n$ mode shape matrix. $\ddot{\mathbf{Y}}_{\mathbf{n}\times 1}$ is the $n\times 1$ modal acceleration response.

In practice, the measurement of a complete structural acceleration response is limited due to the number and location of accelerometers; a reduced-order representation of the measured acceleration response is approximately calculated as follows:

$$\ddot{\mathbf{x}}_{\mathbf{r}\times 1} = \Phi_{\mathbf{r}\times\mathbf{s}}\ddot{\mathbf{Y}}_{\mathbf{s}\times 1}, \tag{28}$$

in which $\ddot{\mathbf{x}}_{\mathbf{r}\times 1} = [\ddot{\mathbf{x}}_1 \ \ddot{\mathbf{x}}_2 \ \cdots \ \ddot{\mathbf{x}}_{\mathbf{r}}]^{\mathbf{T}}$ is the measured acceleration response and the element $\ddot{\mathbf{x}}_{\mathbf{i}}$ ($\mathbf{i} = 1, 2, \ldots, \mathbf{r}$) denotes the acceleration response at the ith DOF. $\ddot{\mathbf{Y}}_{\mathbf{s}\times 1} = [\ddot{\mathbf{Y}}_1 \ \ddot{\mathbf{Y}}_2 \ \cdots \ \ddot{\mathbf{Y}}_{\mathbf{s}}]^{\mathbf{T}}$ is the modal acceleration and $\ddot{\mathbf{Y}}_{\mathbf{j}}$ ($\mathbf{j} = 1, 2, \ldots, \mathbf{s}$) denotes the jth modal acceleration. $\Phi_{\mathbf{r}\times\mathbf{s}} = \begin{bmatrix} \varphi_{11} & \varphi_{12} & \cdots & \varphi_{1\mathbf{s}} \\ \varphi_{21} & \varphi_{22} & \cdots & \varphi_{2\mathbf{s}} \\ \vdots & \vdots & \ddots & \vdots \\ \varphi_{\mathbf{r}1} & \varphi_{\mathbf{r}2} & \cdots & \varphi_{\mathbf{rs}} \end{bmatrix}$ is the mode shape matrix.

Based on (28), the modal acceleration response can be approximately calculated from the measured acceleration response with the generalized inverse of the mode shape matrix $\Phi_{\mathbf{r}\times\mathbf{s}}$ as follows:

$$\begin{aligned} \ddot{\mathbf{Y}}_{\mathbf{s}\times 1} &= \Phi^{+}_{\mathbf{r}\times\mathbf{s}}\ddot{\mathbf{x}}_{\mathbf{r}\times 1}, \\ \ddot{\mathbf{Y}}_{\mathbf{s}\times 1} &= \Phi^{-1}_{\mathbf{r}\times\mathbf{s}}\ddot{\mathbf{x}}_{\mathbf{r}\times 1} \quad (\text{if } \mathbf{r} = \mathbf{s}). \end{aligned} \tag{29}$$

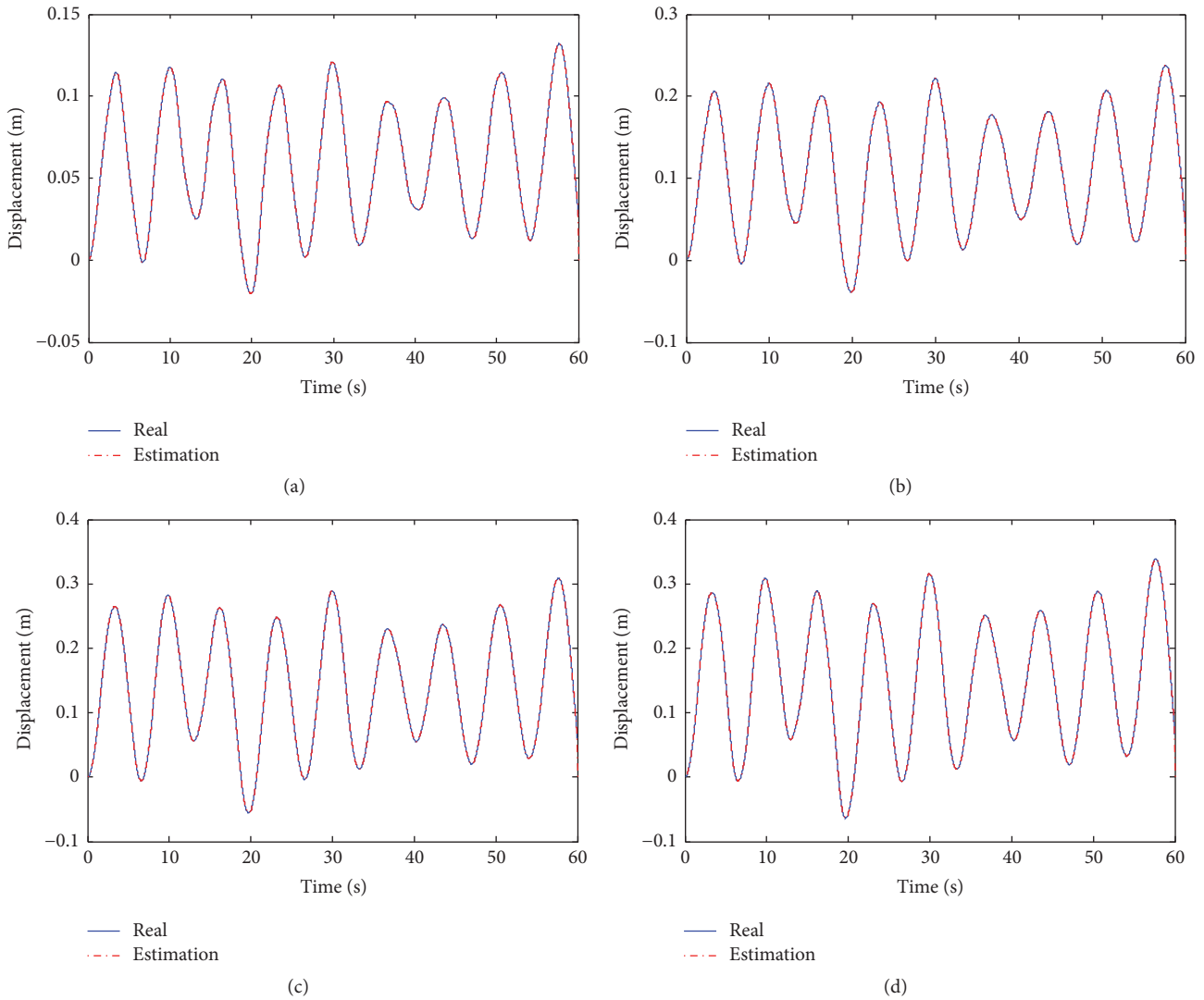

FIGURE 3: Comparison of time histories of structural displacement responses. (a) On the 5th floor; (b) on the 10th floor; (c) on the 15th floor; (d) on the 20th floor.

The error between the estimated and the exact modal acceleration responses can be minimized by choosing the number of the accelerometers to exceed the number of the modes governing the response of the structure.

Based on (27), (1) can be rewritten in modal space as follows:

$$\mathbf{M}_s \ddot{\mathbf{Y}}_{s\times 1}(t) + \mathbf{C}_s \ddot{\mathbf{Y}}_{s\times 1}(t) + \mathbf{K}_s \mathbf{Y}_{s\times 1}(t) = \mathbf{f}(t), \tag{30}$$

where $\mathbf{M}_s = \Phi_{n\times s}^{T} \mathbf{M} \Phi_{n\times s}$, $\mathbf{C}_s = \Phi_{n\times s}^{T} \mathbf{M} \Phi_{n\times s}$, $\mathbf{K}_s = \Phi_{n\times s}^{T} \mathbf{K} \Phi_{n\times s}$, and $\mathbf{f}(t) = \Phi_{n\times s}^{T} \mathbf{F}(t)$ are modal mass, modal damping, modal stiffness, and modal wind load, respectively. $\Phi_{n\times s}$ is the first s mode shape matrix.

The state vector and output vector in modal space can be represented as

$$\begin{aligned} \mathbf{Z}(\mathbf{t}) &= \left[\mathbf{Y}(\mathbf{t}) \quad \dot{\mathbf{Y}}(\mathbf{t})\right]^{\mathbf{T}}, \\ \mathbf{y}(\mathbf{t}) &= \ddot{\mathbf{Y}}(\mathbf{t}). \end{aligned} \tag{31}$$

The state space equation and the measurement equation in modal space can be shown as

$$\begin{aligned} \mathbf{Z}_{k+1} &= \mathbf{A}_k \mathbf{Z}_k + \mathbf{B}_k \mathbf{f}_k, \\ \mathbf{y}_{k+1} &= \mathbf{D}_{k+1} \mathbf{Z}_{k+1} + \mathbf{G}_{k+1} \mathbf{f}_{k+1} + \mathbf{v}_{k+1}, \end{aligned} \tag{32}$$

where

$$\begin{aligned} \mathbf{A}_k &= \left(\mathbf{I}_{2s\times 2s} + \Delta \mathbf{t} \begin{bmatrix} 0_{s\times s} & \mathbf{I}_{s\times s} \\ -\mathbf{M}_s^{-1}\mathbf{K}_s & -\mathbf{M}_s^{-1}\mathbf{C}_s \end{bmatrix} \right), \\ \mathbf{B}_k &= \Delta \mathbf{t} \begin{bmatrix} 0_{s\times s} \\ -\mathbf{M}_s^{-1} \end{bmatrix}, \\ \mathbf{D}_{k+1} &= \left[-\mathbf{M}_s^{-1}\mathbf{K}_s \quad -\mathbf{M}_s^{-1}\mathbf{C}_s\right], \\ \mathbf{G}_{k+1} &= \left[-\mathbf{M}_s^{-1}\right]. \end{aligned} \tag{33}$$

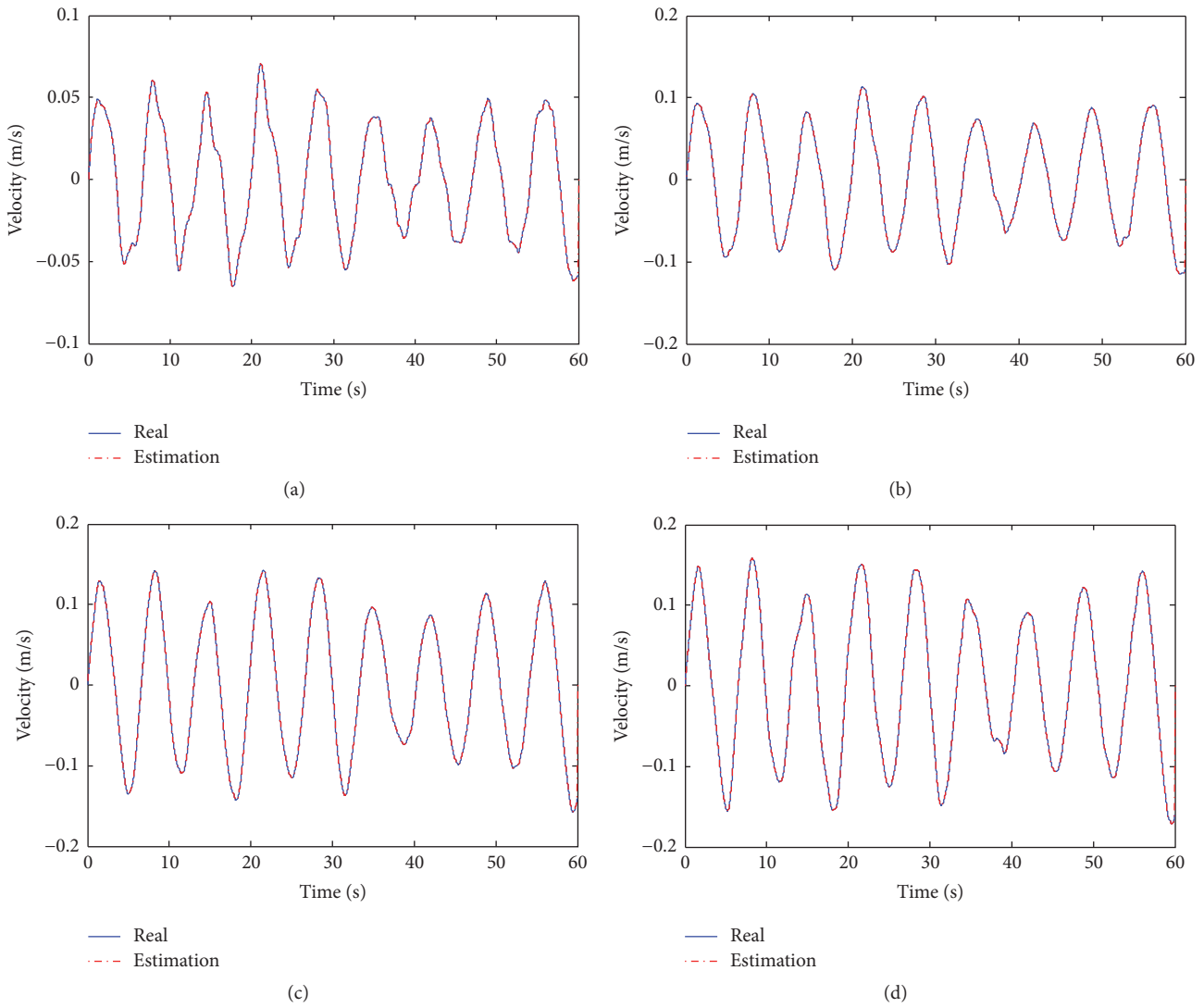

Figure 4: Comparison of time histories of structural velocity responses. (a) On the 5th floor; (b) on the 10th floor; (c) on the 15th floor; (d) on the 20th floor.

Based on the estimation procedure presented in Section 2.1, the first s modal wind load $\mathbf{f}(t)$ can be identified from the modal acceleration response.

Then, the time-varying wind load can be obtained as

$$\mathbf{F}(\mathbf{t}) = \left(\Phi_{\mathbf{n\times s}}^{\mathbf{T}}\right)^{+} \widehat{\mathbf{f}}(\mathbf{t}), \tag{34}$$

where $(\Phi_{\mathbf{n\times s}}^{\mathbf{T}})^{+} = \Phi_{\mathbf{n\times s}}(\Phi_{\mathbf{n\times s}}^{\mathbf{T}}\Phi_{\mathbf{n\times s}})^{-1}$. $\widehat{\mathbf{f}}(\mathbf{t})$ is the identified modal wind load.

3. Numerical Verification

In this section, a twenty-story shear building structure is simulated and studied as an example to investigate the feasibility and reliability of the proposed method. The story height of each floor is 4.8 m. The mass and stiffness of each story are 50 tons and 7500 kN/m, respectively. The damping ratio of the building is assumed to be 0.47%.

In this numerical investigation, the fluctuating wind speed is simulated according to the autoregressive model approach and the spectral density used to simulate the fluctuating wind speed is Davenport spectrum. The time step of the simulated fluctuating wind speed is 0.1 s. The vertical wind profile is taken as the power law and the exponent α is set to be 0.22. The reference height is 10 m according to the Chinese National Load Code [1] and the mean wind speed is 10 m/s at the reference height. The time histories of the simulated fluctuating wind speed on the 5th, 10th, 15th, and 20th floor for a 10 min interval are shown in Figure 1. Figure 2 shows the corresponding comparison of the power spectral density of the simulated fluctuating wind speed with the Davenport spectrum. It can be obtained that the simulated power spectrum density matches very well the Davenport spectrum. To calculate the wind load, the drag coefficient of the structure μ_s is assumed to be 1.6. The density of air is set to be 1.23 kg/m^3. The wind direction is assumed to be perpendicular to the

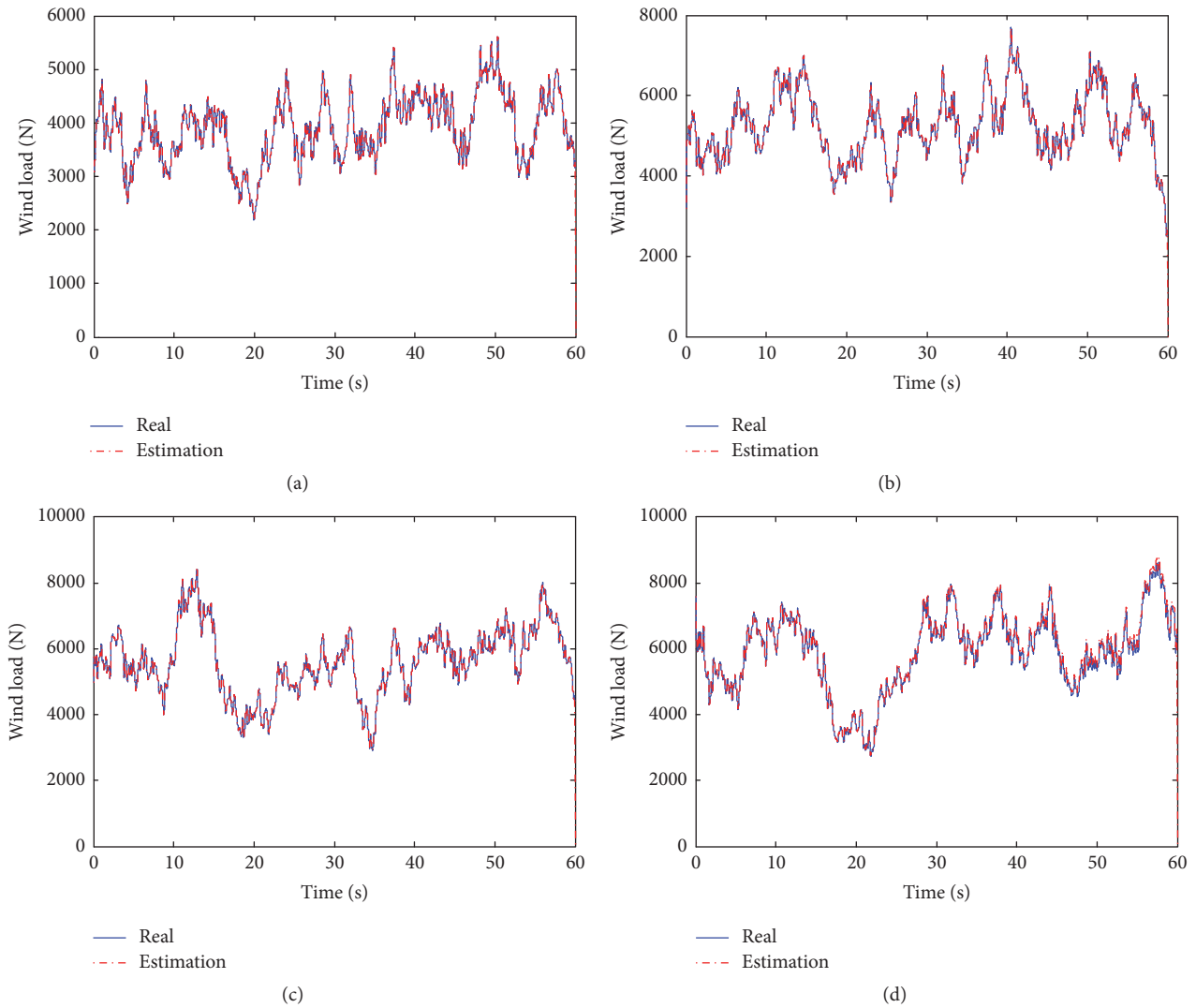

Figure 5: Comparison of time-varying wind load on the building. (a) On the 5th floor; (b) on the 10th floor; (c) on the 15th floor; (d) on the 20th floor.

windward side of the structure. The orthogonal exposed wind area A_s of each floor is assumed to be 24 m^2. For the wind load time histories calculated, refer to the Appendix.

3.1. Wind Load Identification. In this section, the acceleration responses at each story taken as the "measurements" are simulated from the theoretically computed quantities based on Newmark-β method and superimposed with 2% RMS white noise. The initial value of the state vector $\mathbf{Z}_0$ is set to be $[0, 0, 0, \ldots, 0, 0, 0]_{40\times1}$. The initial error covariance matrix $\mathbf{P}_{\mathbf{Z},0}$ of the state vector $\mathbf{Z}_0$ is assumed to be $\mathbf{I}_{40\times40}$. The covariance matrix $\mathbf{R}$ of the measurement noise vector $\mathbf{v}(t)$ is chosen to be $\mathbf{I}_{20\times20}$. The comparisons of the exact and estimated values of state vectors including structural velocity responses and displacement responses on the 5th, 10th, 15th, and 20th floor are shown in Figures 3 and 4, respectively. It can be seen that the estimation results agree well with the exact values. Figure 5 presents the comparison of the identified and exact time-varying wind load on the 5th, 10th, 15th, and 20th floor. It can be observed that the identified wind loads are in good agreement with the exact ones. The mean value and standard deviation of identified errors of the wind load on each floor are tabulated in Table 1; results show that the maximum values of the mean value and standard deviation are 0.58% and 0.38%, respectively. This means that the proposed method has a good approximation capability and the estimation results are accurate.

3.2. The Effect of the Number of Sensors. In practical engineering, measurement of the acceleration response on each DOF is infeasible due to the limited number of accelerometers. To investigate the effect of the number of sensors on the performance of the developed method, wind load on the shear building structure is estimated based on different numbers of accelerometers. Figure 6 illustrates the comparison of the estimated wind loads on the 5th, 10th, 15th, and 20th floor for different numbers of sensors. The number of sensors and corresponding locations are shown in Table 2. In Figure 6, it

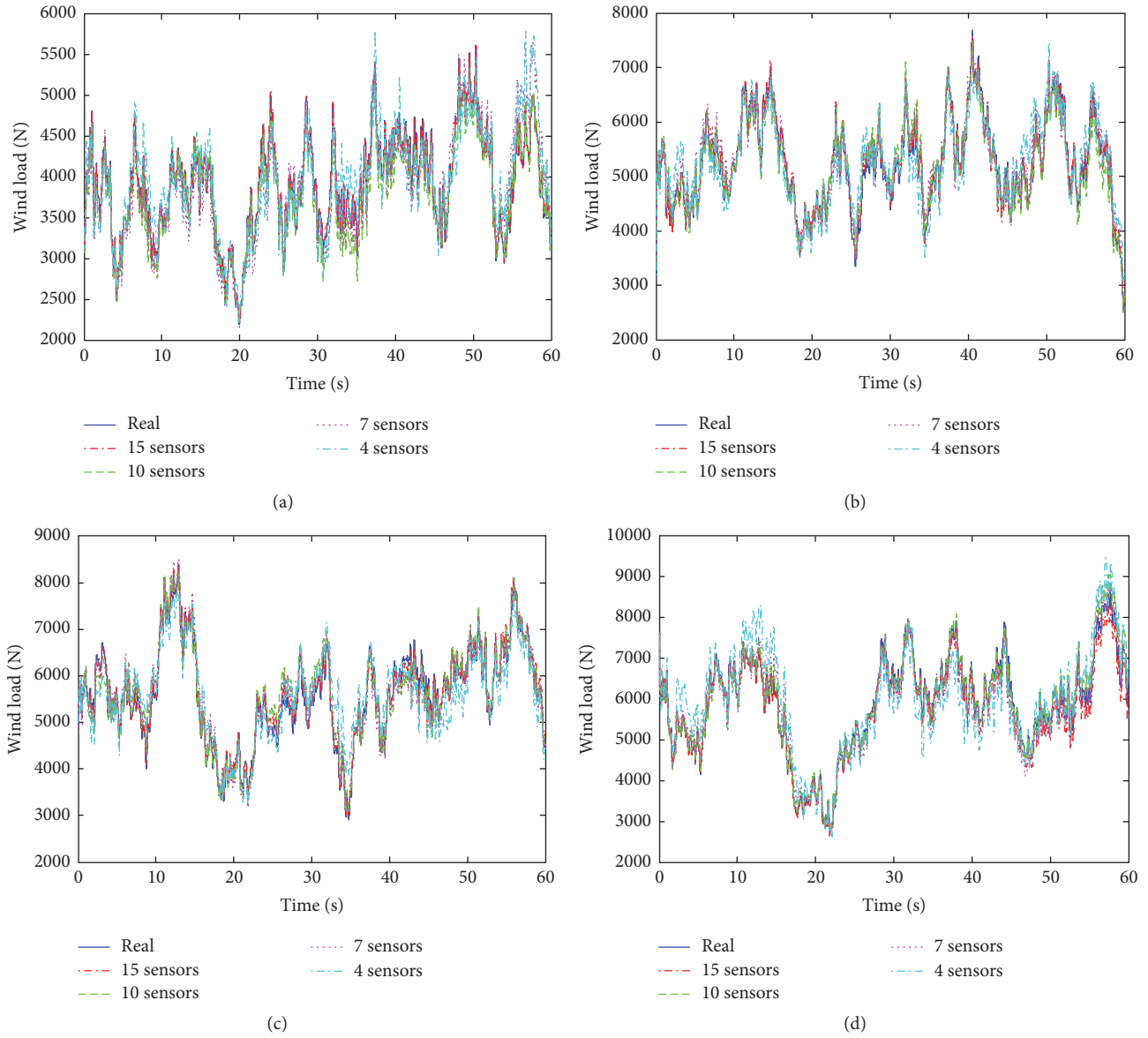

FIGURE 6: The time histories of the estimated wind load for different numbers of sensors. (a) On the 5th floor; (b) on the 10th floor; (c) on the 15th floor; (d) on the 20th floor.

can be seen that the variation trends of the estimated wind load curves are identical to the exact ones. Table 3 gives the errors of the identified wind load with the number of sensors from 4 to 20. Results indicate that, with the increase in the number of sensors, the estimation accuracy is improved. Meanwhile, the average error can be less than 5% when only using seven sensors in this example.

3.3. Sensitivity to Sensor Location. In order to investigate the effect of sensor location, wind load is identified with different sensor distributions. Table 4 shows three types of sensor locations with the number of sensors taken as seven. The estimated wind loads on the 5th, 10th, 15th, and 20th floor with three conditions of sensor locations are illustrated in Figure 7. As shown in Figure 7, it can be found that the estimated wind loads match very well the exact values and the difference of the three estimated curves is slight. It should be noted that the sensors are almost uniformly distributed in these three cases. Through study, the accuracy of the identification results will be affected if the sensors are centrally installed on several floors. Therefore, in order to reduce the estimation errors, the sensors should be uniformly distributed along the height.

3.4. Sensitivity to Structural Modal Parameters. In practical engineering, the structural parameters cannot be determined directly. In general, the finite element model or the parameter identification method is employed to determine the structural parameters. Previous studies show that the accuracy of the identified parameters will be affected by measurement

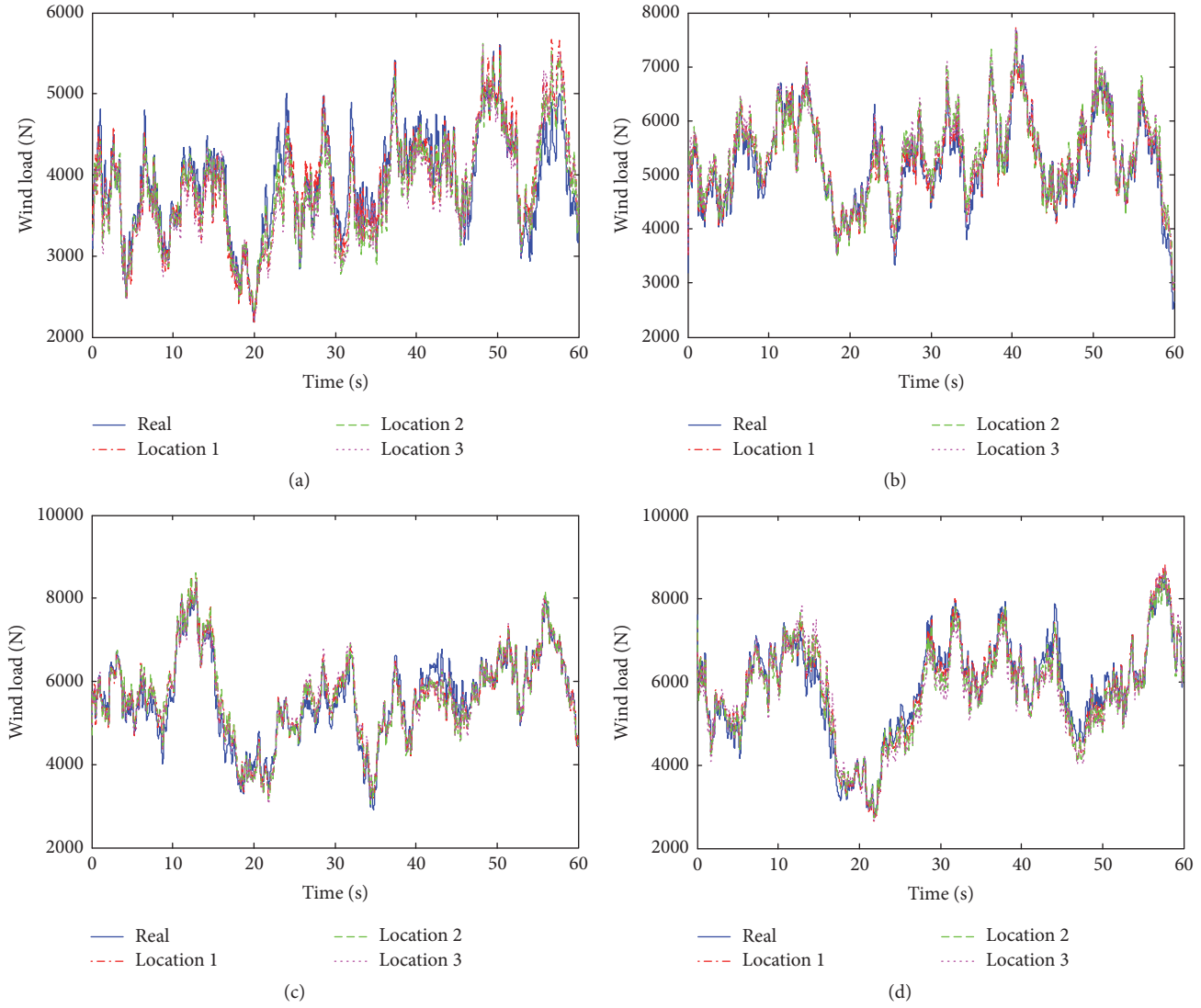

Figure 7: The time histories of the estimated wind load for different types of sensor location. (a) On the 5th floor; (b) on the 10th floor; (c) on the 15th floor; (d) on the 20th floor.

noise, estimation uncertainties, modeling error, and changing environmental conditions [24–28]. There are obvious errors between the artificially determined parameters and the exact values. In this section, the effects of the errors in structural modal parameters on wind load identification are studied. The number of sensors is seven and the location of sensors is the same as Location 1 given in Table 4.

In order to study the effect of natural frequency, the errors in all the natural frequencies are set to be ±5%. Figure 8 compares the estimated wind load with the exact wind load on the 5th, 10th, 15th, and 20th floor for ±5% errors in natural frequencies. It can be observed that there are some differences between the identified time-varying wind loads and the exact ones. The mean value and standard deviation of errors for wind load identification with −5% errors and +5% errors in natural frequencies are listed in Tables 5 and 6, respectively. It can be observed that the mean value and standard deviation of the error are under 9.10% and 7.37%, respectively. It is concluded that the wind load estimation method is sensitive to the error in natural frequencies. Nevertheless, results show that the accuracy of time-varying wind load with ±5% errors in natural frequencies can still satisfy the requirements of engineering application.

For damping ratio errors of ±10%, the identified time histories of wind loads are compared with the exact loads on the 5th, 10th, 15th, and 20th floor in Figure 9. It can be seen that the estimated time-varying wind load curves are in good agreement with those of the exact wind loads. Tables 7 and 8 give the identified errors of the wind load on each floor with −10% errors and +10% errors in damping ratio, respectively, which show that the mean value of the errors on each floor is under 6% and the standard deviation of the errors on each floor is under 5%. The accuracy is close to the case where the damping ratio is exact. It is noticable that the error of the

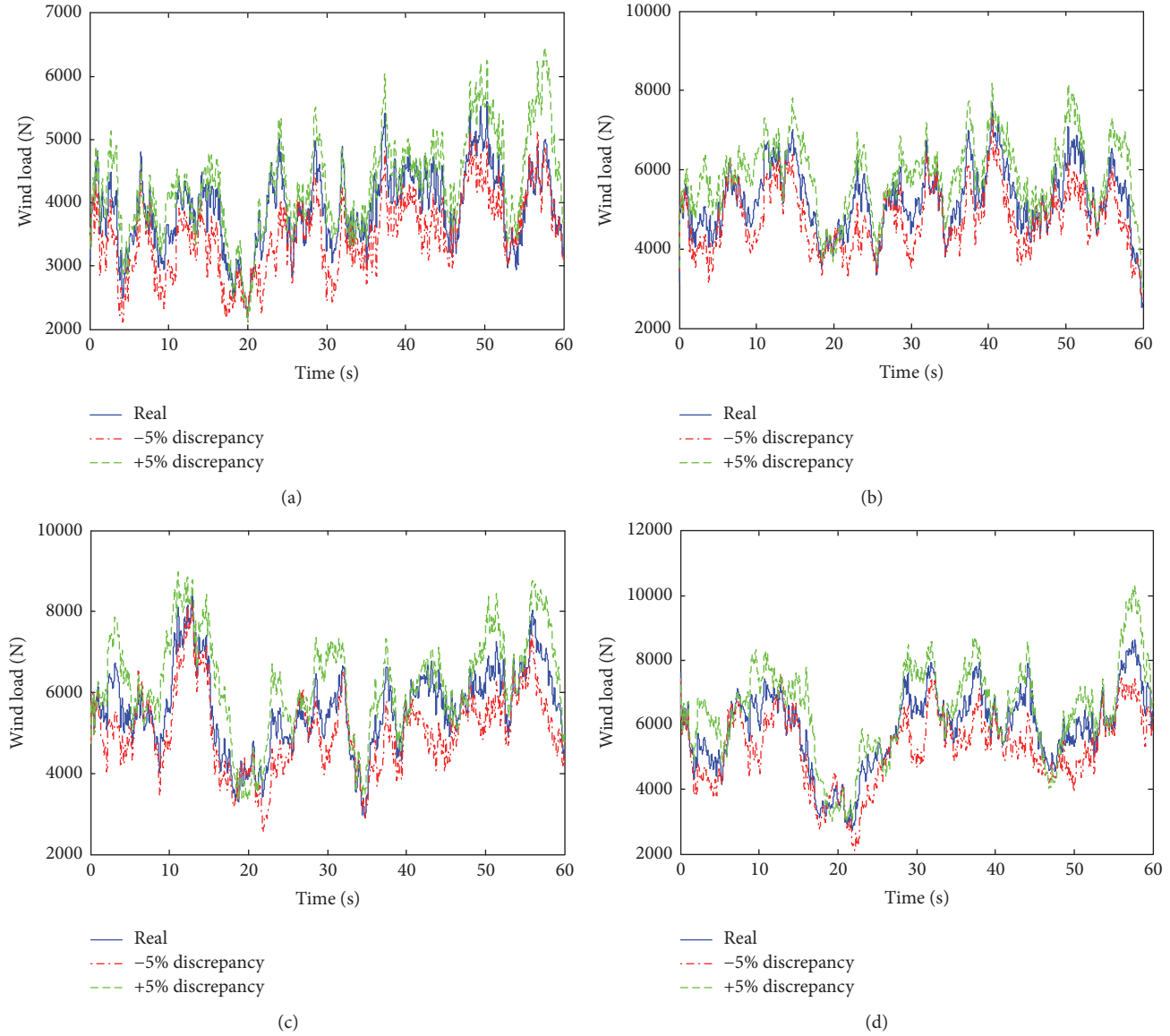

Figure 8: The histories of the estimated wind load with ±5% discrepancy in natural frequencies. (a) On the 5th floor; (b) on the 10th floor; (c) on the 15th floor; (d) on the 20th floor.

damping ratio has a little effect on the estimation accuracy and the inverse method presented in this study is not sensitive to the error in the damping ratio.

4. Conclusion

In this study, an inverse approach based on minimum-variance unbiased estimation is developed for identifying the time-varying wind load from structural acceleration responses. The recursive procedure includes three parts: time update, estimation of unknown wind load, and measurement update. The accuracy and reliability of the proposed method in identifying the time-varying wind load are verified by numerical results of the simulation of a 20-story shear building. Results show that the estimated time-varying wind load and the unknown structural responses are in good agreement with the exact values.

The comparative studies indicate that the wind load can be identified accurately if the number of accelerometers is reduced and the estimation accuracy is improved with the increase in the number of sensors. The accuracy of the identified wind load is slightly influenced by the location of sensors under the condition that the sensors are uniformly distributed along the height. The stability and robustness of the proposed method are verified by estimating the wind load with errors in structural modal parameters. Results show that the proposed method is more sensitive to the error in natural frequency than that for damping ratio. Nevertheless, the errors of the identified results with ±5% errors in natural frequency are still in a reasonable range. Hence, it is

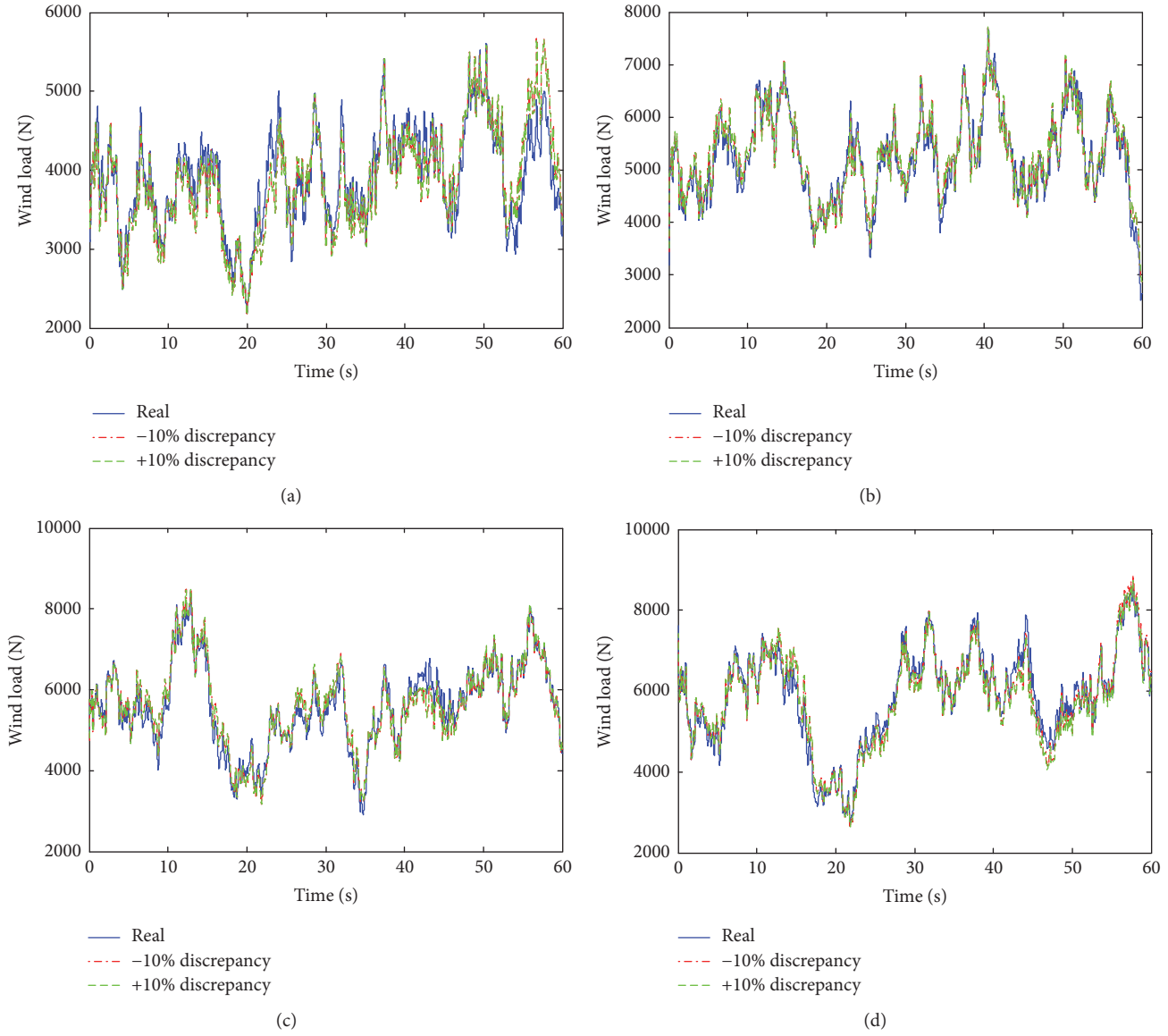

Figure 9: The histories of the estimated wind load with ±10% discrepancy in damping ratio error. (a) On the 5th floor; (b) on the 10th floor; (c) on the 15th floor; (d) on the 20th floor.

concluded that the inverse method developed in this study can be an effective approach for wind load estimation based on limited measurement of structural acceleration response.

Appendix

In this study, only the longitudinal wind load is considered. The transverse and vertical wind loads are neglected. Then, at time t, the wind speed at level z denoted as $u(z,t)$ can be expressed as follows:

$$u(z,t) = \overline{u}(z) + \widehat{u}(z,t), \tag{A.1}$$

in which $\overline{u}(z)$ is the average wind speed at level z; $\widehat{u}(z,t)$ is the fluctuating wind speed at level z, and it varies over time. The average wind speed can be calculated based on the power law as follows:

$$\overline{u}(z) = \overline{u}(z') \left(\frac{z}{z'}\right)^{\alpha}, \tag{A.2}$$

where z' is the reference height and $\overline{u}(z')$ is the average wind speed at the reference height; z and $\overline{u}(z)$ are the arbitrary height and its corresponding average wind speed; α is the power law exponent which can be determined from the terrain condition.

Based on (A.1), the wind pressure at level z can be obtained:

$$\begin{aligned} w(z,t) &= \frac{1}{2}\varrho u^2(z,t) \\ &= \frac{1}{2}\varrho \overline{u}^2(z) + \frac{1}{2}\varrho\left[\widehat{u}^2(z,t) + 2\overline{u}(z)\,\widehat{u}(z,t)\right] \end{aligned}$$

Table 1: The mean value and standard deviation of errors for wind load identification.

Floor number	Mean value (%)	Standard deviation (%)	Floor number	Mean value (%)	Standard deviation (%)
1	0.10	0.09	11	0.07	0.05
2	0.11	0.10	12	0.10	0.06
3	0.12	0.09	13	0.11	0.77
4	0.09	0.08	14	0.08	0.06
5	0.09	0.07	15	0.15	0.10
6	0.10	0.07	16	0.08	0.06
7	0.74	0.06	17	0.12	0.09
8	0.12	0.08	18	0.11	0.09
9	0.07	0.06	19	0.09	0.07
10	0.08	0.05	20	0.58	0.38

Table 2: Number of sensors and corresponding locations.

Number of sensors	Sensor locations (floor)
15	2, 4, 5, 6, 7, 9, 10, 11, 12, 14, 15, 16, 17, 19, 20
10	3, 4, 6, 8, 10, 12, 14, 16, 18, 20
7	3, 6, 9, 12, 15, 18, 20
4	5, 10, 15, 20

Table 3: Mean value of error with different numbers of sensors.

Number of sensors	Average error (%)	Number of sensors	Average error (%)
20	0.84	11	3.53
19	1.27	10	4.24
18	1.83	9	4.30
17	2.23	8	4.44
16	2.59	7	4.81
15	2.60	6	5.67
14	2.84	5	6.08
13	3.04	4	7.21
12	3.10	—	—

Table 4: Number of sensors and corresponding locations.

Number of sensors	Sensor locations (floor)
7	Location 1: 3, 6, 9, 12, 15, 18, 20
7	Location 2: 2, 5, 8, 11, 14, 17, 20
7	Location 3: 1, 4, 7, 10, 13, 16, 19

$$= \overline{w}(z) + \widehat{w}(z,t), \tag{A.3}$$

in which ϱ is the density of air; $\overline{w}(z)$ is the average wind pressure at level z which can be expressed as $\overline{w}(z) = (1/2)\varrho\overline{u}^2(z)$; $\widehat{w}(z,t)$ is the fluctuating wind pressure at level z, and it can be calculated by $\widehat{w}(z,t) = (1/2)\varrho[\widehat{u}^2(z,t) + 2\overline{u}(z)\widehat{u}(z,t)]$.

Table 5: The mean value and standard deviation of errors for the estimated wind load with −5% error in natural frequencies.

Floor number	Mean value (%)	Standard deviation (%)	Floor number	Mean value (%)	Standard deviation (%)
1	7.50	2.25	11	6.42	5.77
2	7.32	3.49	12	7.87	6.10
3	3.50	4.04	13	7.13	6.10
4	5.29	4.40	14	6.73	6.25
5	6.67	4.61	15	6.60	6.52
6	5.56	5.07	16	6.85	6.64
7	6.67	5.29	17	6.98	6.64
8	6.38	5.15	18	7.44	6.66
9	5.26	5.61	19	6.68	6.90
10	6.00	5.67	20	7.26	7.23

Table 6: The mean value and standard deviation of errors for the estimated wind load with +5% error in natural frequencies.

Floor number	Mean value (%)	Standard deviation (%)	Floor number	Mean value (%)	Standard deviation (%)
1	8.21	2.41	11	8.76	6.09
2	8.39	3.70	12	8.82	6.47
3	8.32	4.27	13	8.94	6.45
4	8.43	4.64	14	8.90	6.64
5	8.36	4.87	15	9.00	6.91
6	8.60	5.35	16	9.09	7.04
7	8.70	5.59	17	9.10	7.05
8	8.54	5.43	18	9.03	7.08
9	8.74	5.93	19	9.03	7.37
10	8.74	5.98	20	7.18	6.59

Table 7: The mean value and standard deviation of errors for the estimated wind load with −10% error in damping ratio.

Floor number	Mean value (%)	Standard deviation (%)	Floor number	Mean value (%)	Standard deviation (%)
1	5.71	4.28	11	4.24	2.98
2	5.89	3.28	12	3.89	3.27
3	5.08	4.63	13	3.93	3.13
4	4.82	3.74	14	5.59	3.65
5	4.87	2.79	15	3.72	2.88
6	3.20	3.77	16	5.46	3.38
7	4.77	4.17	17	4.82	3.71
8	5.95	3.07	18	3.98	3.64
9	3.55	2.27	19	4.31	2.87
10	2.95	2.98	20	3.52	2.74

Table 8: The mean value and standard deviation of errors for the estimated wind load with +10% error in damping ratio.

Floor number	Mean value (%)	Standard deviation (%)	Floor number	Mean value (%)	Standard deviation (%)
1	5.62	5.23	11	4.24	3.01
2	5.79	3.31	12	3.87	3.23
3	5.14	4.65	13	3.91	3.13
4	4.81	4.77	14	5.56	3.65
5	4.83	3.70	15	3.71	2.85
6	3.20	2.78	16	5.58	3.40
7	4.77	3.74	17	4.87	3.69
8	5.84	4.05	18	3.96	3.62
9	3.67	3.15	19	4.26	2.71
10	2.99	2.30	20	3.74	2.91

The wind load at level z can be calculated as

$$F(z,t) = \mu_s(z) A_s(z) w(z,t), \quad (A.4)$$

where $\mu_s(z)$ is the drag coefficient of the structure at level z; $A_s(z)$ is the windward area of the structure at level z.

Conflicts of Interest

The authors declare that there are no conflicts of interest regarding the publication of this article.

Acknowledgments

This work was financially supported by the Science & Technology Foundation of Shenzhen, China (Grant no. JCYJ20170413105418298).

References

[1] X. Jin, J. Wang, M. Gu et al., *Load Code for the Design of Building Structures*, China Architecture & building press, Beijing, China, 2012.

[2] D. Williams and R. P. N. Jones, "Dynamic loads in aeroplanes under given impulsive loads with particular reference to landing and gust loads on a large flying boat," *Aeronautic Research Council*, no. 2221, 1948.

[3] J. C. Briggs and M.-K. Tse, "Impact force identification using extracted modal parameters and pattern matching," *International Journal of Impact Engineering*, vol. 12, no. 3, pp. 361–372, 1992.

[4] Y.-B. Yang and J.-D. Yau, "Vehicle-bridge interaction element for dynamic analysis," *Journal of Structural Engineering*, vol. 123, no. 11, pp. 1512–1518, 1997.

[5] J. Sanchez and H. Benaroya, "Review of force reconstruction techniques," *Journal of Sound and Vibration*, vol. 333, no. 14, pp. 2999–3018, 2014.

[6] X. Q. Jiang and H. Y. Hu, "Reconstruction of distributed dynamic loads on an Euler beam via mode-selection and consistent spatial expression," *Journal of Sound and Vibration*, vol. 316, no. 1–5, pp. 122–136, 2008.

[7] M. C. Djamaa, N. Ouelaa, C. Pezerat, and J. L. Guyader, "Reconstruction of a distributed force applied on a thin cylindrical shell by an inverse method and spatial filtering," *Journal of Sound and Vibration*, vol. 301, no. 3–5, pp. 560–575, 2007.

[8] E. Jacquelin, A. Bennani, and P. Hamelin, "Force reconstruction: analysis and regularization of a deconvolution problem," *Journal of Sound and Vibration*, vol. 265, no. 1, pp. 81–107, 2003.

[9] E. Zhang, J. Antoni, and P. Feissel, "Bayesian force reconstruction with an uncertain model," *Journal of Sound and Vibration*, vol. 331, no. 4, pp. 798–814, 2012.

[10] U. Güntürkün, "Sequential reconstruction of driving-forces from nonlinear nonstationary dynamics," *Physica D. Nonlinear Phenomena*, vol. 239, no. 13, pp. 1095–1107, 2010.

[11] C.-K. Ma, J.-M. Chang, and D.-C. Lin, "Input forces estimation of beam structures by an inverse method," *Journal of Sound and Vibration*, vol. 259, no. 2, pp. 387–407, 2003.

[12] S. S. Simonian, "Inverse problems in structural dynamics. I. Theory," *International Journal for Numerical Methods in Engineering*, vol. 17, no. 3, pp. 357–365, 1981.

[13] S. S. Simonian, "Inverse problems in structural dynamics–II. Applications," *International Journal for Numerical Methods in Engineering*, vol. 17, no. 3, pp. 367–386, 1981.

[14] J. Chen and J. Li, "Study on wind load inverse of tall building," *Chinese Quarterly of Mechanics*, vol. 22, no. 1, pp. 72–77, 2001.

[15] C. C. Kang and C. Y. Lo, "An inverse vibration analysis of a tower subjected to wind drags on a shaking ground," *Applied Mathematical Modelling*, vol. 26, no. 4, pp. 517–528, 2002.

[16] S. S. Law, J. Q. Bu, and X. Q. Zhu, "Time-varying wind load identification from structural responses," *Engineering Structures*, vol. 27, no. 10, pp. 1586–1598, 2005.

[17] J.-S. Hwang, A. Kareem, and W.-J. Kim, "Estimation of modal loads using structural response," *Journal of Sound and Vibration*, vol. 326, no. 3–5, pp. 522–539, 2009.

[18] J.-S. Hwang, A. Kareem, and H. Kim, "Wind load identification using wind tunnel test data by inverse analysis," *Journal of Wind Engineering and Industrial Aerodynamics*, vol. 99, no. 1, pp. 18–26, 2011.

[19] M. Klinkov and C. P. Fritzen, "Wind load observer for a 5MW wind energy plant," in *Proceeding of the IMAC-XXVIII*, Conference Proceedings of the Society for Experimental Mechanics Series, pp. 719–726, Florida, FL, USA, 2010.

[20] L.-H. Zhi, M.-X. Fang, and Q. S. Li, "Estimation of wind loads on a tall building by an inverse method," *Structural Control and Health Monitoring*, vol. 24, no. 4, Article ID e1908, 2017.

[21] L.-H. Zhi, B. Chen, and M.-X. Fang, "Wind load estimation of super-tall buildings based on response data," *Structural Engineering and Mechanics*, vol. 56, no. 4, pp. 625–648, 2015.

[22] S. Gillijns and B. De Moor, "Unbiased minimum-variance input and state estimation for linear discrete-time systems," *Automatica*, vol. 43, no. 1, pp. 111–116, 2007.

[23] S. Gillijns and B. De Moor, "Unbiased minimum-variance input and state estimation for linear discrete-time systems with direct feedthrough," *Automatica*, vol. 43, no. 5, pp. 934–937, 2007.

[24] S. Alampalli, "Effects of testing, analysis, damage, and environment on modal parameters," *Mechanical Systems and Signal Processing*, vol. 14, no. 1, pp. 63–74, 2000.

[25] B. Moaveni, J. P. Conte, and F. M. Hemez, "Uncertainty and sensitivity analysis of damage identification results obtained using finite element model updating," *Computer-Aided Civil and Infrastructure Engineering*, vol. 24, no. 5, pp. 320–334, 2009.

[26] B. Goller and G. I. Schuëller, "Investigation of model uncertainties in Bayesian structural model updating," *Journal of Sound and Vibration*, vol. 330, no. 25, pp. 6122–6136, 2011.

[27] J. Ching and J. L. Beck, "Bayesian analysis of the phase II iasc - asce structural health monitoring experimental benchmark data," *Journal of Engineering Mechanics*, vol. 130, no. 10, pp. 1233–1244, 2004.

[28] T. Haukaas and P. Gardoni, "Model uncertainty in finite-element analysis: bayesian finite elements," *Journal of Engineering Mechanics*, vol. 137, no. 8, pp. 519–526, 2011.